Optimization of Piezoelectric Energy Harvester with Line-Regulation

Ibtisam Aziz[1]*, Tariq Mahmood[1], Wahaj Rafique[2] and Ali Raza[2]

[1] Department of Electrical Engineering, Institute of Space Technology (IST), Islamabad Pakistan

[2] Department of Mechanical Engineering, National University of Technology(NUTECH), Islamabad

***Correspondence**: ibtisamazizist@gmail.com

Highlights

- An efficient scheme of Piezoelectric Energy Harvesting.
- DC-DC boost converter with Line regulation.
- Applications include self-powered electronic devices.

Received date: 2025-09-03

Accepted date: 2025-12-20

Published date: 2025-02-28

Abstract: Stair based Piezoelectric energy harvester (SBPH) is proposed to be placed in the footstep of stairs to harvest clean energy using the applied force. A system, independent of external power supply is developed which has the capability to charge a mobile phone. To reduce the loading effect, 90 Piezoelectric pressure sensors (PPS) in the SBPH are innovatively connected in parallel combination using Schottky diodes. A wooden art that consists of a network of 86 springs and 4 fasteners is used to concentrate the applied force on the anode of each PPS. A battery of 3.7 V at 3700 mAh can be charged through the SBPH. Moreover, the current system has the ability to efficiently utilize the harvested energy stored in the battery, using DC-DC converter with line regulation. Line regulation is achieved with TL494 Integrated chip (IC) as well as an Arduino UNO. The line regulation circuit based on Arduino has also a distinctive feature to disconnect the battery from the electronic circuit, when walking activity stops for a longer period of time. This system is cost effective and can be used in crowded places such as metro stations, airports, and so forth.

Keywords: Piezoelectric energy harvesting, Clean Energy, DC-DC converter, Line regulation, Footstep, Battery storage.

1. Introduction

Every second, our sun produces enough energy to sustain Earth's needs for 500,000 years. Mankind just needs to grasp these Renewable energy sources (RES) and utilize them in the best efficient way. It wouldn't be out of place to say that the modern world is dependent on energy.

Energy requirement is increasing rapidly with the decrease in conventional sources for power generation[1, 2], thus the trends of energy generation are changing day by day [3, 4]. To fulfill this requirement, there are conventional and non-conventional methods for energy generation. Conventional method includes the energy generation using fuel (petrol, coal [5, 6], gas[7] and so forth). They give Carbon dioxide (CO2) as the byproduct [8, 9, 10], thus affecting the environment [11, 12] and health [13]. Non-conventional ways include energy generation through renewable sources (RS) such as solar energy [14, 15], hydel energy [16] as the largest source of renewable energy in the world [17], wind energy [18, 19, 20], geothermal energy [21] and so forth. Many conventional and non-conventional resources are used to meet this requirement; RES is one of them. Only 23% of the world energy is obtained through RES [4]. In 2018, Global energy demand increased by 2.3%, with more than 600 million people deprived of the electricity. Furthermore, 1.9% increase in CO2 was also observed [22]. Thus, compelling the policy makers to increase the RES (up to 65%), to achieve the target of energy demand by 2050 [23] and to maintain temperature rise below 2◦C according to Paris Climate Agreement [24].

Most of the renewable energy sources have the limitations related to it, such as funding issues, space requirement, low efficiencies, less man power, non-favorable conditions and so forth [25, 26, 27, 28, 29]. Interestingly energy is also associated to the human beings in the form of kinetic energy [30, 31]. Each step taken by the individual results in the waste of energy. Efficient conversion of human movement to electric energy can contribute to renewable energy.

Different techniques and sensors were used to harvest energy with the help of locomotion. Energy can be harvested from motion using electromagnetic harvesters [32, 33, 34, 35, 36], inertial energy harvesters [37, 38] and piezoelectric material [39, 40, 41]. Both Lead zirconate titanate (PZT) [42] and Polyvinylidene fluoride (PVDF) [43] exhibits direct piezoelectric effect [44] and converse piezoelectric effect [45]. When pressure is applied on the effective part of the sensor and voltages are produced across the electrode, it is known as the direct effect. On the contrary, when deformation is observed in the sensor by applying voltage at the two electrodes, is converse or inverse effect of the piezoelectric sensor [46]. Due to high charge constant of the PZT, it is extensively used in the energy harvesters [47]. Direct effect of the PPS is used to harvest energy from piezoelectric material. Piezoelectric elements were used to harvest energy using the vibrations produced due to the flow [48, 49]. Energy was harvested by the pressure applied by the rain drops [50, 51].[52] utilize the vibrational kinetic energy of the vapors and harvested energy through it. Vibrations produced due to the movement of vehicles on the bridge were converted to electric energy using piezoelectric harvester [53]. Piezoelectric harvester was placed at a specific depth in the road and energy was harvested when the vehicles passed through it. Average power of 1.15 W was achieved while keeping the load resistance 900 Ω [54]. [55] uses piezoelectric harvester to drive an electronic circuit of Light emitting diode (LED) placed in the shoe. Whenever someone walks, the circuit sense the energy harvested and LED is illuminated, resulting in efficient usage of battery. Piezoelectric harvester consisting of PZT, magnets and coil increases the output power by ten times, which is used to light up 99 LEDs [56]. An Internet of things (IOT) based system which collects data of the environment was powered up by the piezoelectric elements placed in the walkway, providing maximum output power 0.12 W [57]. Furthermore, piezoelectric sensor was embedded in the shoe to harvest energy through it [58, 59, 60].Different circuits were used to boost the generated voltages up to the desired requirement with line regulation [61, 62]. [63] uses the boost circuit with piezoelectric energy harvester. Previous work shows that piezoelectric sensors can generate a sufficient amount of energy. [64] Shows that while inclining or declining more pressure is applied by the foot as compared to the ground. In this context, an innovative piezoelectric energy harvester was introduced, placed in the stairs. The system consists of an insulating board on which PPS are placed using Schottky diodes with a wooden art which contains a network of springs and fasteners. A lithium ion battery, 3.7 V at 3700 mAh is charged whenever a step is taken on the piezoelectric harvester. Furthermore, it also consists of an electronic circuit with distinctive features to power up an electronic device. Finally, this paper presents a piezoelectric energy harvester independent of the external power source.

2. Open Circuit Voltage

The maximum output voltage that can be obtained through any source at infinite resistance, when no current is flowing is known as open circuit voltage [65]. Oscilloscope (HMO 1022) is used to measure the open circuit voltage of the PPS because sudden peaks cannot be measured through voltmeter as it has finite internal resistance, thus the values of voltage varies with the variation of internal resistance of voltmeter [66]. The low pass filter function of the oscilloscope is used, to obtain a non-distorted output waveform. Open circuit voltage of the PPS is obtained using the circuit shown in Fig.1(a). Force can be exerted in the form of stress or strain. When force of compression is applied, the electric dipole is induced in the direction of applied force, resulting in positive voltages. On the contrary, when force of tension is applied, the electric dipole is induced opposite to the direction of applied force, resulting in negative voltages. A sinusoidal waveform of 7 Peak to Peak voltage (Vpp) is obtained when either of the actions take place as shown in Fig.1(b).Output voltages and currentsMaximum output voltage is obtained using the circuit displayed in Fig.1(a), as the resistance is infinite. Practical loads are not infinite, therefore variable R2 was used to achieve the trend followed by the output voltages. Different combinations such as single PPS, two PPS in series and two PPS in parallel were used to obtain the output voltages using the experimental model and circuit schematic displayed in Fig.1(c) and Fig.1(d) respectively. Equivalent circuit of the PPS consist of a current source (Ipz), Capacitor (Cpz) and resistor (Rpz) [67] as depicted in Fig.1(d). To minimize systematic and human errors, average of 16 attempts were taken using the oscilloscope by applying pressure of 60 KPa and the values were tabulated in Table 1. Behavior of the output voltage for different combinations with respect to different values of R2 is displayed in Fig.1(e).In order to obtain the current for different combinations, equation 1 is taken in account. Table 1 shows the current values obtained in each case. Vpp for each case was obtained from Table 1. Fig.1(f) shows the trend of the output current for different combinations with respect to different values of R2.

$$I_{pp} = \frac{V_{pp}}{R_2} \qquad (1)$$

To obtain the optimal value of power harvested by the PPS, maximum power transfer curve is obtained using the voltage and current values in Table 1. The maximum power transfer curve for different combination was obtained using Equation 2.

$$P = V\ I \qquad (2)$$

Fig.1(g) shows the graphs for maximum power transfer curve. The maximum power transfer point is 35 mW at 3.2 KΩ in case of single PPS shown in g(i), 40.89 mW at 1000 Ω when 2 PPS are connected in series shown in g(ii) and 52.92 mW at 322 Ω in case of 2 PPS connected in parallel shown in g(iii). Therefore, PPS were connected in parallel to get the optimum power.

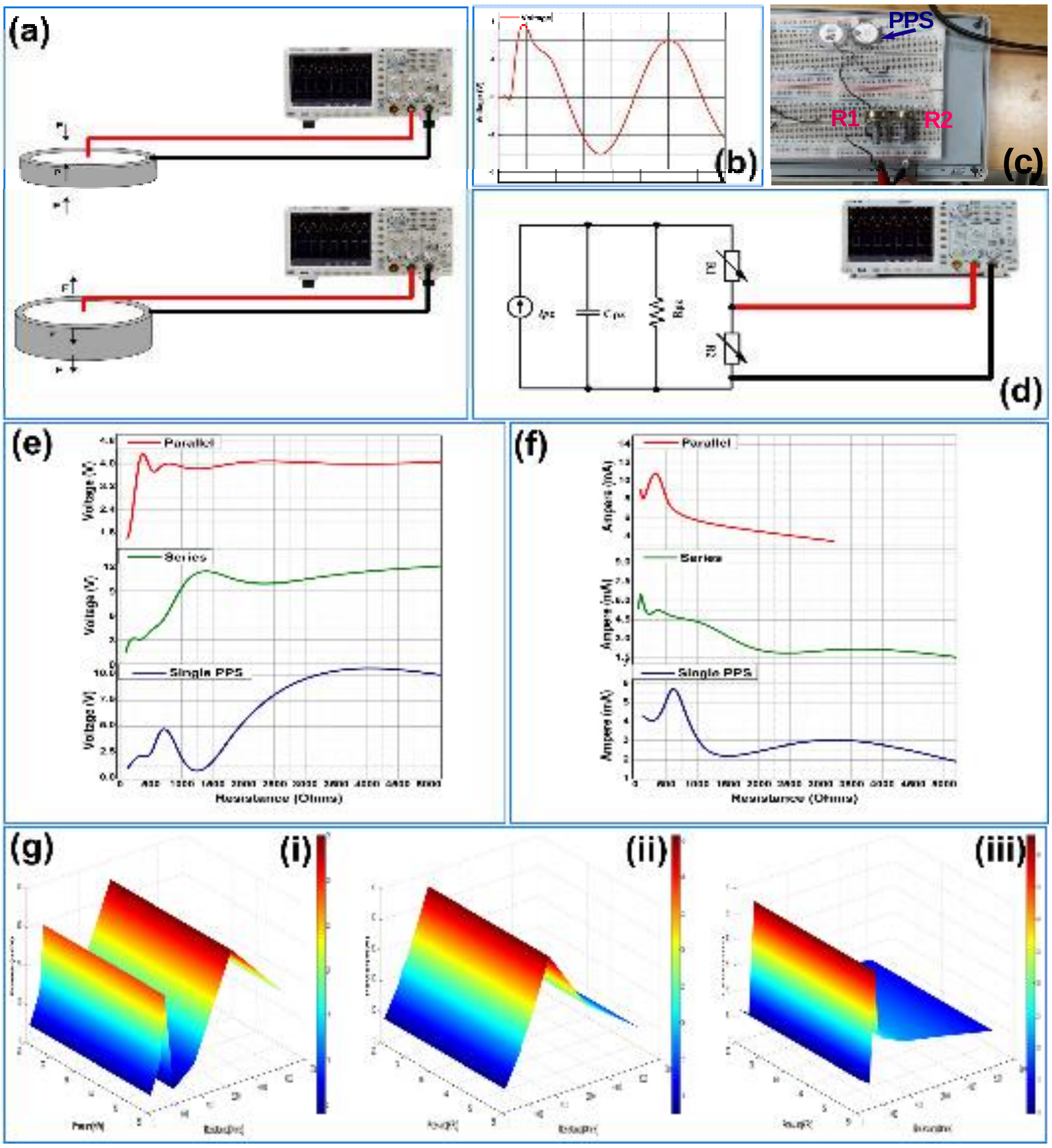

Figure 1: (a) Force of compression and tension applied on the PPS with the output taken using Oscilloscope.(b) Open circuit voltage (V) waveform of single PPS.(c) Experimental model to obtain the output voltages with different values of resistance(R2).(d) Schematic diagram to obtain the output voltages with different values of

resistance(R2).(e) Trends of voltage for different combinations of PPS.(f) Trends of current for different combinations of PPS.(g) Maximum power transfer curves:(i) for single PPS, (ii) PPS connected in series,(iii) PPS connected in parallel.

3. Proposed design for Piezoelectric energy harvester

3.1 Loading effect

According to the maximum power transfer curves displayed in Fig 1(g), more power could be obtained when the PPS were connected in parallel rather than in series. 90 PPS, placed on a board were connected in parallel.

Table 1: Values of voltage (V), current (mA) and power(mW) at various resistances R(Ω) for different combinations of PPS

	Resistance (Ω)	Voltage (V)	Current (mA)	Power (mW)
PPS	120	1	4.3	4.3
	322	2.2	3.8	8.36
	500	2.5	5	12.5
	650	4.5	6.5	29.2
	1000	2	2	4
	1800	4	2.2	8.8
	3200	10	3.5	35
	5200	10	1.92	19.2
PPS in series	90	1.4	6.5	9.1
	120	2.2	5.97	13.1
	322	3	5.2	15.6
	500	4.12	4.98	20.5
	650	5	4.72	23.6
	1000	9.4	4.35	40.8
	1800	10.5	2.45	25.7
	3200	10.6	2.13	22.5
	5200	12	1.56	18.8
PPS in parallel	90	1.4	9	12.6
	120	1.4	7	9.8
	322	4.2	12.6	52.9
	500	3.8	7.6	28.8
	650	3.89	6.6	25.6
	1000	3.9	5.56	21.6
	1800	4	4.67	18.7
	3200	4.03	3.45	13.9

To check the output of the insulating board, pressure of 60–80 KPa was applied on it and an electrolytic capacitor of 0.1 F was charged through the schematic circuit depicted in Fig 2(a), its experimental model is displayed in Fig.2(b). Fig.2(c) displays the board on which 90 PPS are connected in parallel. The capacitor charges up to 2.9 V but the rise time was very slow due to small amount of current harvested from the PPS. To increase the current, diodes were used with each PPS connected in parallel shown in Fig.2(d), thus reducing the loading effect. Schottky diodes (0.3 V) were considered instead of Silicon diodes (0.7 V), to minimize their effect on the output voltages. 0.1 F capacitor was directly charged using the output of the PPS, the capacitor was charged till 4.5 V, with the major improvement in rise time. The value of current for each of the case is calculated using equation 3.

$$I = \frac{CV}{T} \tag{3}$$

Current value of 0.375 A was obtained when Schottky diodes were taken in account, while on the contrary current value obtained was 0.193 A. Addition of Schottky diodes increased the current value by 0.182 A.

3.2 Design Concept

The proposed design for the SBPH, intends to convert the mechanical pressure applied by the foot to an electrical energy. It consists of an insulating board having dimensions (10” x 11” x 0.08”). 90 PPS are stacked on it through epoxy and connected in parallel using Schottky diodes as shown in Fig.3(a). It is observed that to increase the efficiency of the PPS, force must be concentrated on the anode (effective part) of each sensor. A wooden art of identical dimensions as insulating board is displayed in Fig.3(b) with a network of 86 springs and 4 fasteners, placed orthogonal to the board containing PPS, making the springs exactly at right angle to the anode of each sensor. Springs have been added to the wooden art in such a way that they halt over the sensors and keep striking them even after the exerted pressure is removed for an instant, resulting in optimum output. The exploded view of the SBPH is shown in Fig.3(c).

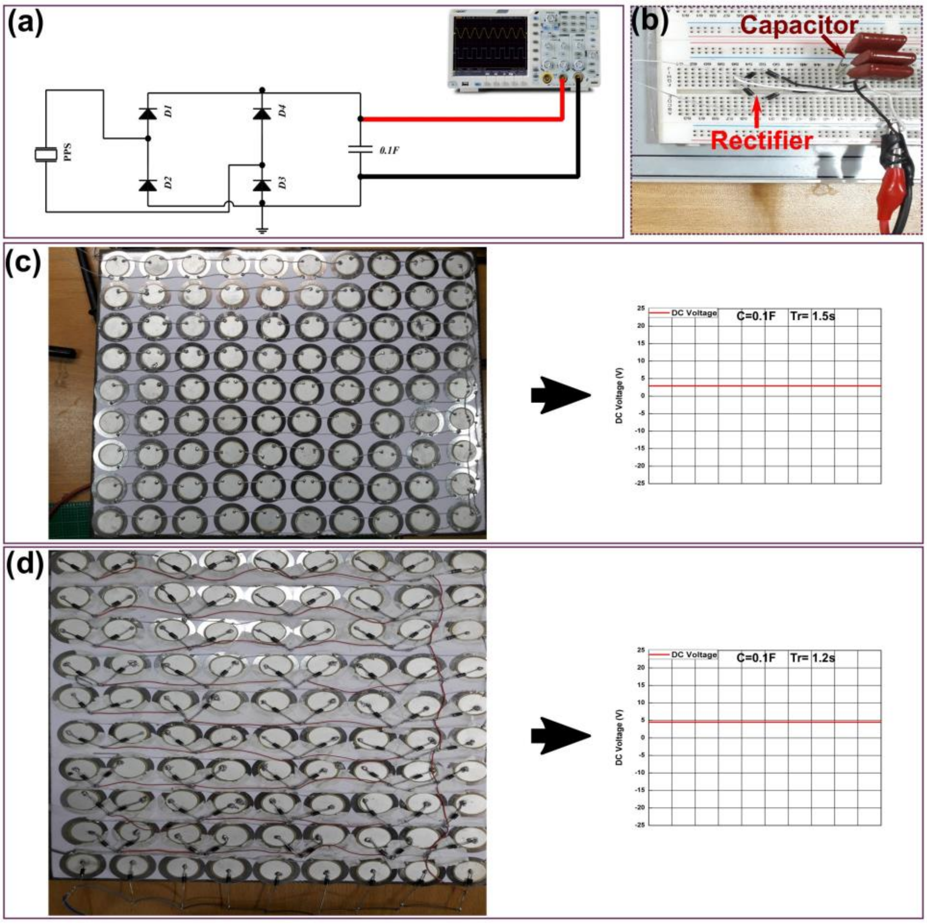

Figure 2: (a) Schematic diagram to charge 0.1 F capacitor. (b) Experimental model to charge 0.1 F Capacitor. (c) 0.1 F Capacitor charged up to 2.9 V with 90 PPS connected in parallel. (d) 0.1 F Capacitor charged up to 4.5 V with 90 PPS connected in parallel through Schottky diodes.

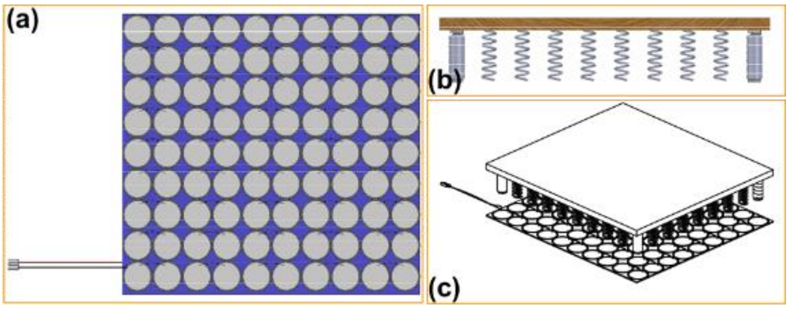

Figure 3: (a) Insulated board containing 90 PPS connected in parallel through Schottky diodes.(b) side-view of the wooden art with 86 springs and 4 fasteners.(c) Exploded view of the SBPH.

To show the concentration of force on the PPS, static structural analysis is performed. Mesh for the SBPH is generated as depicted in Fig.4(a). Equivalent (von-mises) stress is shown in Fig.4(b), which makes it evident that the applied force is only concentrated on the PPS, thus making the design concept efficient.

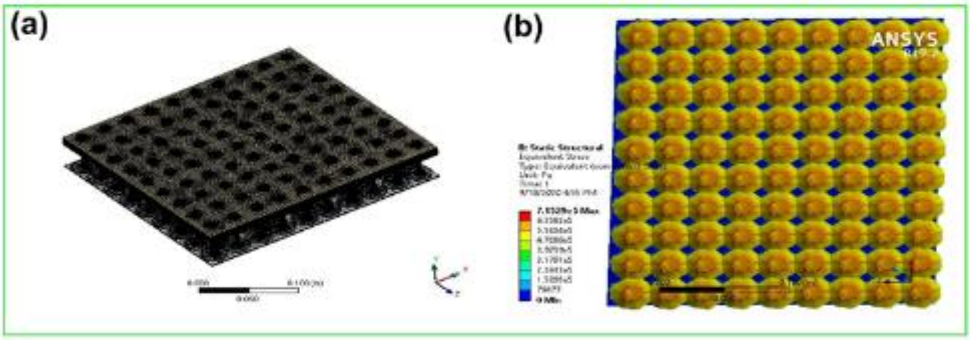

Figure 4: (a) Generated mesh for the SBPH.(b) Distribution of stress on the 90 PPS.

The proposed system consists of a single tile and aims to be placed below the stairs where the pressure of the foot is maximum. The most suitable place would be a Bus station, metro station and so forth, where frequent movements of people are observed. This results in the continuous energy.

3.3 Control Circuit

Efficient storage and usage of energy are of equal importance as its generation. Power electronics has played a major role in this regard. The parallel combination of PPS used in the SBPH gives the output between 1.4-4.5 V depending upon the intensity of force applied to the SBPH. For optimal usage of the energy generated through the SBPH, boost converters are used with distinctive features.

3.4 Mathematical Calculation for Boost Circuit

$$
\begin{aligned}
&V_O = 5\ V\\
&I_O = 1\ A\ (Can\ vary\ practically)\\
&V_{in} = 1.4 - 3.7\ V\ \ (Input\ to\ the\ boost\ circuit)\\
&f = 35\ KHz\\
&Now\ for\ V_{in} = 1.4\ V\\
&D = 1 - \frac{V_S}{V_O} = 1\breve{}\,\frac{1.4}{5} = 0.72\\
&I_L = \frac{V_O I_O}{V_S} = 3.57\ A\\
&Let\ 40\%\ variation\ in\ inductor\ current\\
&We\ have\\
&dI_L = 0.4(3.57) = 1.42\ A\\
&L = \frac{V_S D}{dI_L f} = 0.0202\ mH\\
&Now\ for\ 3.7\ V\\
&D = 1 - \frac{V_S}{V_0} = 1\breve{}\,\frac{3.7}{5} = 0.26\\
&I_L = \frac{V_0 I_0}{V_S} = 1.351\ A\\
&Let\ 40\%\ variation\ in\ inductor\ current\\
&We\ have\\
&dI_L = 0.4(1.351) = 0.54\ A\\
&L = \frac{V_S D}{dI_L f} = 0.0508\ mH\\
&now\\
&dI_L = \frac{V_S D}{Lf} = \frac{(1.4)(0.72)}{(50.8\times10^{-6})(35\times10^{3})} = 0.566\ A\\
&I_{Lmax1.4V} = I_L + \frac{dI_L}{2} = 3.57 + \frac{0.566}{2} = 3.853\ A\\
&I_{Lmax3.7V} = I_L + \frac{dI_L}{2} = 1.351 + \frac{0.566}{2} = 1.634\ A
\end{aligned}
$$

Inductor being the most important storage element, plays a major role in the output of the converters. 0.2456 mm,30 AWG wire is wrapped around the 2-inch ferrite core to make an inductor of resistance equal to 5.14 Ω as shown in Fig.5(a). Schematic of the boost converter is depicted in Fig.5(b). Feedback circuit for load regulationOutput of the boost converter is regulated at 5 V, since the mobile battery is charged at fixed voltage level. Output is regulated by two method generation through the SBPH. The output of the SBPH is given to 3.7 V at 3700 mAh Lithium battery. The battery voltages are boosted using DC-DC converter to charge an electronic device.

3.5 Feedback circuit for load regulation

Output of the boost converter is regulated at 5 V, since the mobile battery is charged at fixed voltage level. Output is regulated by two methods.

3.5.1 Using TL494 IC

TL494 IC shown in Fig.5(c) is a pulse width modulated IC. It consists of the feedback path, which is used to obtain the feedback from the load and provide it to the IC, varying the pulse width of the generated square wave. Thus, regulating the output voltage of the boost converter. TL494 IC consists of two amplifiers, voltage error amplifier and current error amplifier. It also includes an oscillator; its frequency is adjusted with the help of RT and CT using equation 4.

$$F_{osc} = \frac{1}{R_T * C_T} \tag{4}$$

Output of the oscillator and error amplifiers are compared using comparator which accordingly generates the square wave with the frequency equals to Fosc=35.12 kHz (when RT =1.8 kΩ and CT =15 nF). Although, duty cycle depends on both the inputs to the comparator. If both inputs are same then the output of error amplifier will be zero, else the difference is amplified. This input is given to the comparator within the IC, another input of comparator is given through oscillator as depicted in Fig.5(d). Thus, the comparison gives the output in the form of square wave which is fed back to the gate of Metal-oxide Semiconductor Field-effect Transistor (MOSFET) used in the boost converter and accordingly changes the duty cycle which regulates the output. Fig.5(e) shows the schematic circuit of the boost circuit with line regulation achieved using TL494 IC.

Waveforms of inductor current, generated square wave of F=35.12 kHz and input to the gate of MOSFET are shown in Fig.5(f), Fig.5(g) and Fig.5(h), respectively.

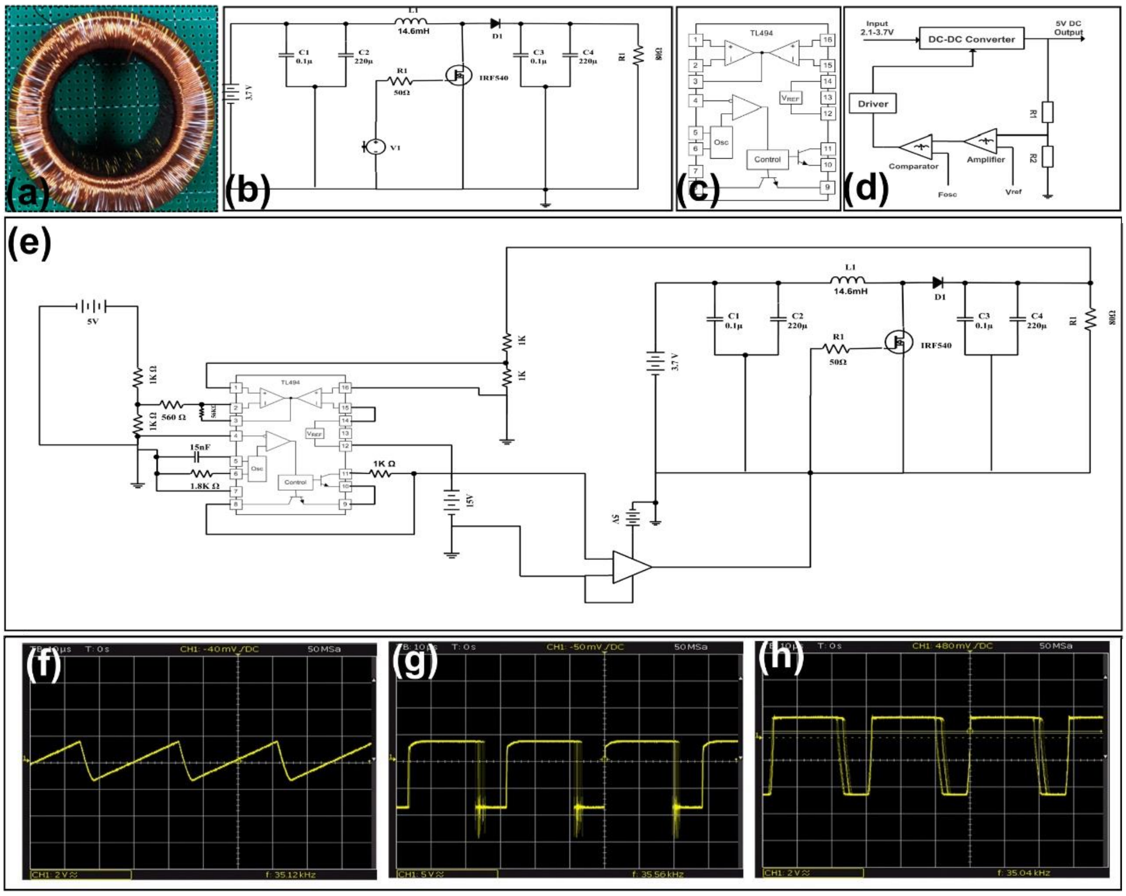

Figure 5: (a) Inductor (L). (b) schematic diagram of DC-DC Boost converter. (c) TL494 IC. (d)Block diagram to achieve line regulation. (e) Circuit diagram of Boost converter with line regulation using TL494 IC. (f) Waveform of the Inductor current. (g) Square wave(F=35 KHz) generated by TL494 IC. (h) Input given at the gate of MOSFET.

3.5.2 Using Arduino UNO

Circuit schematic of boost circuit with line regulation using Arduino is shown in the Fig.6(a). Output of boost circuit is fed back to Arduino UNO using two 1.2 KΩ resistors. Whenever the input is varied, the output is observed and accordingly Pulse Width Modulation (PWM) through Arduino varies to maintain a constant output voltage. If input increases, PWM decreases and vice versa to keep the output voltages constant. Hence, achieving the line regulation. Line regulation is desired to keep the output voltage constant, when the battery voltages decreases as a result of non-continuous walking activity.

PWM of frequency 31 kHz is generated by Arduino and is fed to the boost converter in order to drive the N-Channel MOSFET (IRF540N). When the battery voltages go below 1.4 V, the Arduino cut off the circuit using P-Channel MOSFET (IRF9640) until the battery voltages are restored. It is an independent control circuitry in which no external power source is used. The battery is charged through the tiles, which power up the rest of the circuit including electronic load. The complete flow process is depicted in Fig.6(b).

4. Experimental results

It is evident from Table 1 that maximum power for the single PPS is achieved at 3.2 KΩ. Theoretically, the maximum power point for 90 PPS in parallel can be achieved at 580 Ω, including resistance of soldering part, flexible wires and Schottky diodes.

To obtain the maximum power point of the SBPH, a person weighting 70kg was stepped over it for different values of resistance using circuit depicted in Fig.1(d). Different values of voltage, current and power was achieved with variable resistance as tabulated in Table 2. The maximum power of1.125 W was practically achieved at 650 Ω.

The force applied by the foot varies from person to person according to their weight. The energy harvested by the SBPH varies with the weight of the person. To obtain values of output power, volunteers from different age groups were selected. The volunteers were divided into 4 categories on the basis of their weight. Each volunteer was asked to step 16 times on the SBPH. Fig.7 shows the power obtained for different categories, while keeping the load resistance 650Ω. The maximum output power of 1.92 W was achieved, when the volunteer having weight 90 kg applied maximum pressure on it as depicted in Fig.7.

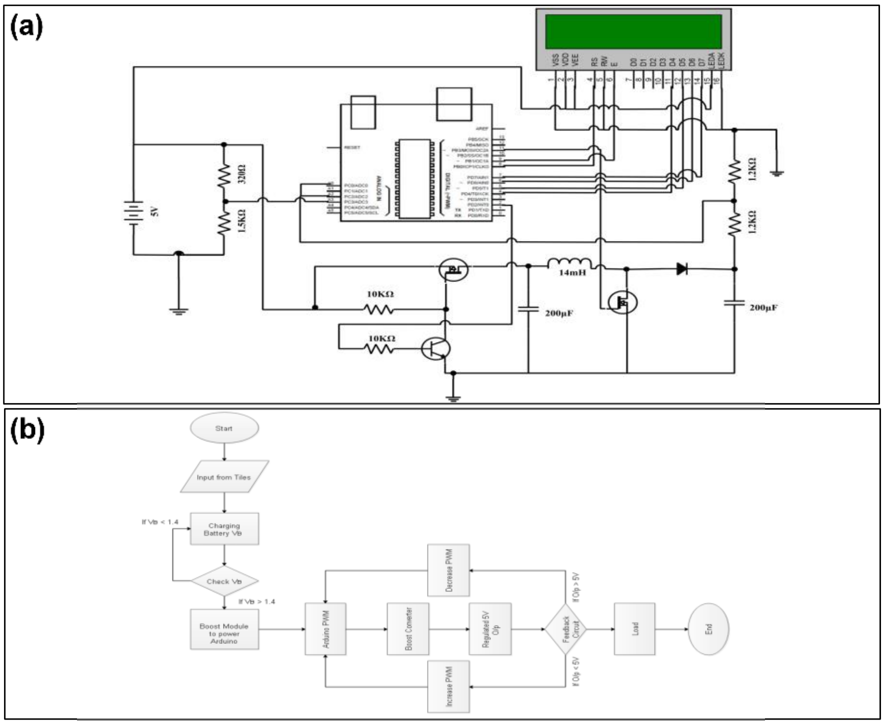

Figure 6: (a) Boost Converter with line regulation using Arduino (UNO). (b) Control flow of the process.

4.1 Prototype of SBPH

Designing the structure for the SBPH, according to the requirement is of key importance. The proposed model as shown in Fig.8(a), having dimensions (10”x11”x1.9”) is designed to be placed under the step of stairs.

Graphically description of the movement of a person is shown in Fig.8(b) where the SBPH is placed under the stairs. A Lithium ion battery is charged through it, which is further given to an electronic circuit to get the desired output for the load to be driven.

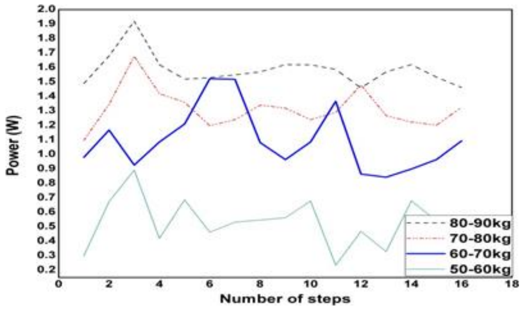

Figure 7: Power (W) harvested for different volunteers with different weight (kg)

Table 2: Value of voltage (V), current (A), and power (W) obtained at various loads (Ω) for volunteer weighting 70 kg

Resistance (Ω)	Voltage (V)	Current (A)	Power (W)
90	1.4	0.37	0.518
120	1.9	0.34	0.652
350	2.6	0.31	0.827
500	3.5	0.28	0.991
650	4.5	0.25	1.125
1000	4.6	0.19	0.874
1800	4.7	0.13	0.611
3200	4.7	0.11	0.517
5200	4.7	0.06	0.282

4.2 Practical implementation

The wooden art when placed over the insulating board, exerts the pressure on the anode of the sensors.

SBPH with the electronic circuit is shown in Fig 9(a). Feedback path is achieved by both ways, using TL494 IC and Arduino UNO. The most preferable is through Arduino, because it makes the system flexible and independent.

4.3 Cost viability

Insignificant number of papers were found with the total cost on energy harvesting system using the footstep method. The cost of an energy harvesting system based on the footstep energy generation was 125 USD [68] with the output power 1.4 W. Cost for the current implemented system including electronic circuit comes to be 30 USD. A decrease of 76% in the total cost is observed while comparing it with the previous work. Similarly, the decrease in cost has minimum effect on the average output power. This makes the current system cheaper than the previous developed systems, based on the footstep power generation.

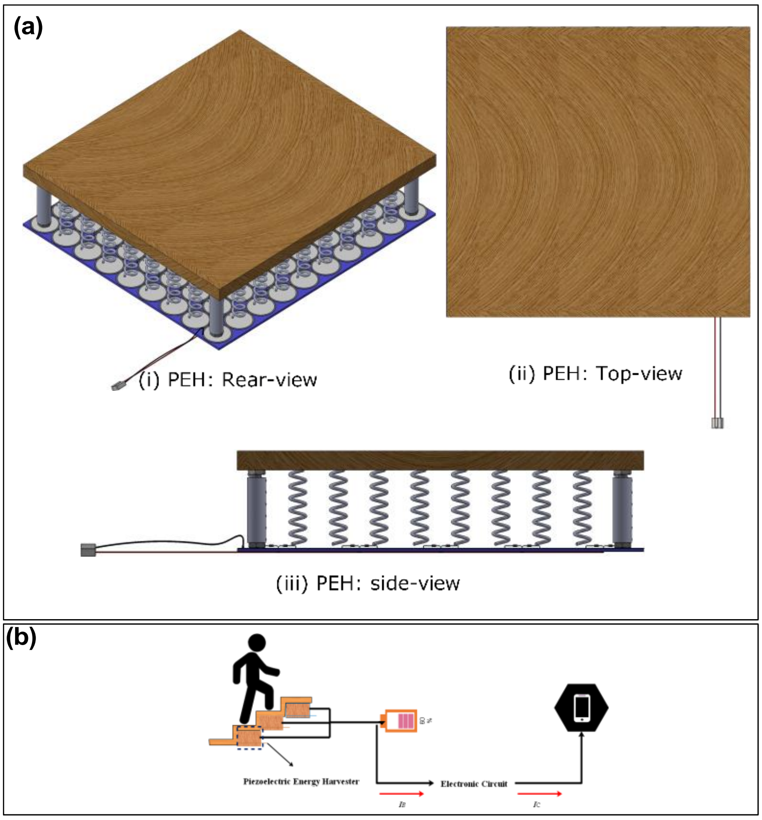

Figure 8: (a) Configuration of SBPH: (i)Rear-view, (ii) Top-view, (iii) Side-view. (b) Graphical description for the setup of SBPH

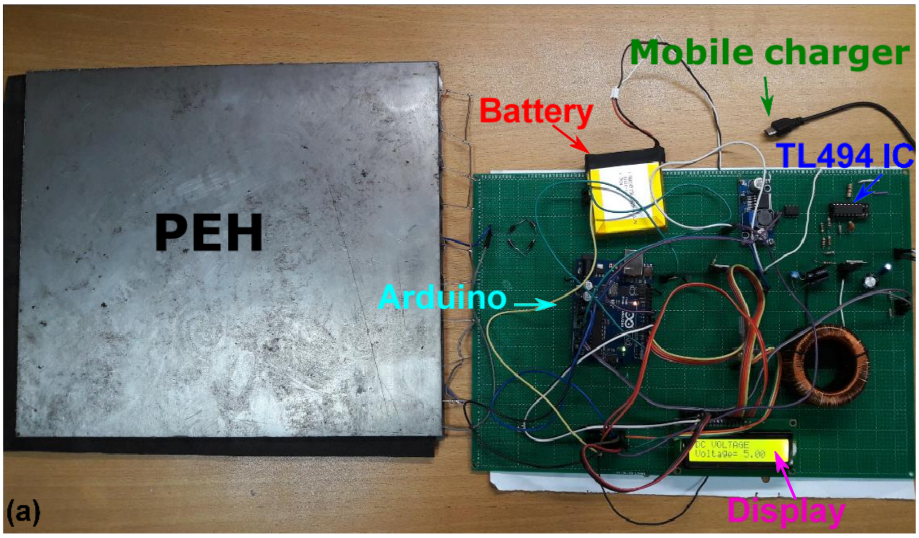

Figure 9: Photograph of the setup that consists of SBPH ,DC-DC converter with line regulation obtained through both(Arduino and TL494 IC) and mobile charger

5. Discussion

It is evident that the researchers are working to develop new ways of energy generation to fulfil the future energy requirement. In this context, Energy has been harvested using the motion of an object. For this purpose, primarily three methods have been used which are electromagnetic harvesters [32, 33, 34, 35, 36], inertial energy harvesters [37, 38] and piezoelectric material harvesters [39, 40, 41]. Due to high output voltage, temperature range and low cost, piezoelectric sensors are preferably used for the purpose of energy harvesting.

The above gives researcher potential area to focus. [48, 50] utilizes piezoelectric sensors to harvest energy from the flow of water and rain drops respectively. Piezoelectric sensors were also embedded in the road to utilize the movement of vehicles for energy generation [54]. Energy was also harvested by placing the piezoelectric sensors in the shoes [58, 59, 60].

There are still some challenges associated with the energy harvested using piezoelectric material. More complex structures have been developed in the previous work, which are not easy to implement. The storage of energy harvested also implies some challenges, which include efficient DC-DC conversion. The focus of this research is on mechanical to electrical conversion illustrated in Fig.8(a) with efficient storage.

This study gives prove of introductory concept of utilizing footstep of the stairs for energy harvesting by placing a novel structure of SBPH within it. Stairs were given preference over the ground because the concentration of foot pressure is maximum at the footstep of stairs. A simpler efficient structure is designed as compared to the complex structures [54, 56, 57] which can be easily implemented and is cost effective. The current system is more efficient than the previous ones due to its storage circuit and unique mechanism of applying pressure at the anode of PPS using the wooden art.

The output of the SBPH depends on the weight and angle with which the foot is placed on the step. Weight of the person has a significant effect on the output of the SBPH due to the difference in the applied force. It has been observed that the output varies from 0.3 W to 1.92 W as the weight changes from 50 kg to 90 kg. This shows a direct relation between the weight and the output. Angle with which the step is taken on the SBPH, effects the output. Maximum output is obtained at 90 degree. A small change in the angle reduces the contact surface and thus decreases the output.

The SBPH is a combination of matrix of PPS and a wooden art, which exerts the pressure on the PPS. From different combinations of the PPS, it was concluded that the power harvested is maximum when the PPS are connected in parallel. Initially two prototypes where tested, 90 PPS in parallel with diodes and without diodes. It was observed that the rise time of the current while charging the capacitor (0.1 F) was low without diodes as compared to with diodes. The SBPH consists of a matrix of 90 PPS connected to each other in parallel through Schottky diodes, to avoid loading effect. The wooden art includes 86 springs and 4 fasteners, designed in such a manner to exert the pressure on the anode of the PPS effectively. The harvested energy is stored in the battery (3.7 V at 3700 mAh), which is boosted upto 5 V to charge an electronic load (mobile phone). The boost circuit has the feature of Line regulation with the capability to disconnect the battery from the circuit when the voltages of the battery reduce below the threshold voltage, as a result of low frequency of walking activity. The output of the proposed system varies with different parameters. Although weight has a significant effect on it. Maximum output obtained is 1.92 Wmax, when a person weighting 90 kg applied maximum foot pressure on it. There is still room for further research in this area. A sandwiched structured of the SBPH can be focused, having layer of PPS above and below the wooden art. Efficiency can be further increased by this way.

6. Conclusion

In this paper, we proposed a harvesting system based on the PPS. A novel design was presented to convert the energy wasted by the human feet to an electrical energy. Main points that were concluded are given below:

- The design of the SBPH consist of a novel wooden art, which helps to efficiently transfer the pressure applied to the PPS. Loading effect of the PPS connected in parallel, is eliminated using Schottky diode (0.3 V), thus increasing the output power.
- The SBPH can generate maximum output power of 1.92 Wmax with maximum voltage of 4.5Vmax when a person weighting 90 kg step on it.
- The current system has the ability to maintain 5V DC output, along with the ability to cut off the battery voltage from the DC-DC converter when the battery voltages goes below the threshold (1.4 V) due to infrequent walking activity.
- The system has the ability to charge a mobile phone in real time.

We believe that the current system is cheaper and efficient to drive small electronic loads. Thus, can contribute to the energy demand of the society. Furthermore, future work in this domain can increase the efficiency of the overall system with decrease in the total cost.

Authorship contribution statement

Ibtisam Aziz: Analysis, Data collection, Drafting the manuscript, Writing – review & editing Tariq Mahmood,Wahaj Rafique and Ali Raza: Design of methodology.

Declaration of competing interest

The authors declare that they have no known competing financial interests or personal relationships that could have appeared to influence the work reported in this paper.

Acknowledgement

This work was carried out under the supervision of Tariq Mahmood at the Institute of Space Technology, Islamabad. His assistance gave much confidence and helped me to endure some difficult times.

Nomenclature

AWG	American Wire Gauge
C	Capacitor
C_T	Capacitor with Oscillator
C_{pz}	PPS Equivalent Capacitor
CO_2	Carbon Dioxide
D	Duty Cycle
dI_L	Change in Inductor Current
f	Frequency
F_{os}	Frequency of Oscillator
I	Current
I_L	Inductor Current
I_{Lmax}	Maximum Inductor Current
I_o	Output Current
I_{pz}	PPS Equivalent Current Source
IC	Integrated Chip
IOT	Internet of Things
L	Inductor
LED	Light Emitting Diode
mAh	milli Ampere Hour
MOSFET	Metal-oxide Semionductor Field-effect Transistor
P	Power
PPS	Piezoelectric Pressure Sensor
PV DF	Polyvinylidene fluoride
PWM	Pulse Width Modulation
PZT	Lead zirconate titanate
R	Resistor
R_T	Resistor with Oscillator
R_{pz}	PPS Equivalent Resistor
RES	Renewable Energy sources
RS	Renewable Sources
SBPH	Stair Based Piezoelectric Energy Harvester
T	Rise Time
USD	United States Dollar
V	Voltage
V_{in}	Input Voltage
V_o	Output Voltage
V_s	Source Voltage
V_{pp}	Peak to Peak Voltage

References

1. Y. Matsuo, A. Yanagisawa, Y. Yamashita, A global energy outlook to 2035 with strategic considerations for asia and middle east energy supply and demand interdependencies, Energy Strategy Reviews 2 (1) (2013) 79–91.
2. T. M. Harris, J. P. Devkota, V. Khanna, P. L. Eranki, A. E. Landis, Logistic growth curve modeling of us energy production and consumption, Renewable and Sustainable Energy Reviews 96 (2018) 46–57.
3. J. L. Aleixandre-Tudó, L. Castelló-Cogollos, J. L. Aleixandre, R. Aleixandre-Benavent, Renew- able energies: Worldwide trends in research, funding and international collaboration, Renewable Energy 139 (2019) 268–278.
4. H.-W. Schiffer, T. Kober, E. Panos, World energy council's global energy scenarios to 2060, Zeitschrift für Energiewirtschaft 42 (2) (2018) 91–102.
5. J. Yuan, C. Na, Q. Lei, M. Xiong, J. Guo, Z. Hu, Coal use for power generation in china, Resources, Conservation and Recycling 129 (2018) 443–453.
6. S. Michalski, D. P. Hanak, V. Manovic, Advanced power cycles for coal-fired power plants based on calcium looping combustion: A techno-economic feasibility assessment, Applied Energy 269 (2020) 114954.

7. B. Odetayo, M. Kazemi, J. MacCormack, W. D. Rosehart, H. Zareipour, A. R. Seifi, A chance constrained programming approach to the integrated planning of electric power generation, natural gas network and storage, IEEE Transactions on Power Systems 33 (6) (2018) 6883–6893.
8. A. K. Karmaker, M. M. Rahman, M. A. Hossain, M. R. Ahmed, Exploration and corrective measures of greenhouse gas emission from fossil fuel power stations for bangladesh, Journal of Cleaner Production 244 (2020) 118645.
9. Q. Yan, Y. Wang, T. Baležentis, Y. Sun, D. Streimikiene, Energy-related co2 emission in china's provincial thermal electricity generation: Driving factors and possibilities for abatement, Energies 11 (5) (2018) 1096.
10. J.-J. Ma, G. Du, B.-C. Xie, Co2 emission changes of china's power generation system: Input- output subsystem analysis, Energy Policy 124 (2019) 1–12.
11. L. Chai, X. Liao, L. Yang, X. Yan, Assessing life cycle water use and pollution of coal-fired power generation in china using input-output analysis, Applied Energy 231 (2018) 951–958.
12. Y. Pu, J. Song, L. Dong, W. Yang, S. Wang, et al., Estimating mitigation potential and cost for air pollutants of china's thermal power generation: A gains-china model-based spatial analysis, Journal of Cleaner Production 211 (2019) 749–764.
13. M. Gao, G. Beig, S. Song, H. Zhang, J. Hu, Q. Ying, F. Liang, Y. Liu, H. Wang, X. Lu, et al., The impact of power generation emissions on ambient pm2. 5 pollution and human health in china and india, Environment international 121 (2018) 250–259.
14. F. M. Guangul, G. T. Chala, Solar energy as renewable energy source: Swot analysis, in: 2019 4th MEC International Conference on Big Data and Smart City (ICBDSC), IEEE, 2019, pp. 1–5.
15. S. Motahhir, A. Chalh, A. El Ghzizal, A. Derouich, Development of a low-cost pv system using an improved inc algorithm and a pv panel proteus model, Journal of Cleaner production 204 (2018) 355–365.
16. B. Guo, B. Xu, D. Chen, W. Ye, P. Guo, X. Luo, Dynamic modeling and energy distribu- tion analysis in a hydroelectric generating system considering the stochastic turbine flow, International Journal of Electrical Power & Energy Systems 103 (2018) 611–621.
17. M. Bilgili, H. Bilirgen, A. Ozbek, F. Ekinci, T. Demirdelen, The role of hydropower installations for sustainable energy development in turkey and the world, Renewable Energy 126 (2018) 755–764.
18. V. Jahangiri, C. Sun, Integrated bi-directional vibration control and energy harvesting of monopile offshore wind turbines, Ocean Engineering 178 (2019) 260–269.
19. J. Wang, Y. Xu, M. Lv, Modeling and simulation analysis of hybrid energy storage system based on wind power generation system, in: 2018 International Conference on Control, Automation and Information Sciences (ICCAIS), IEEE, 2018, pp. 422–427.
20. J. Li, X. B. Yu, Onshore and offshore wind energy potential assessment near lake erie shoreline: a spatial and temporal analysis, Energy 147 (2018) 1092–1107.
21. R. Archer, Geothermal energy, in: Future Energy, Elsevier, 2020, pp. 431–445.
22. R. Newell, D. Raimi, G. Aldana, Global energy outlook 2019: The next generation of energy, Resources for the Future (2019) 8–19.
23. D. Gielen, F. Boshell, D. Saygin, M. D. Bazilian, N. Wagner, R. Gorini, The role of renewable energy in the global energy transformation, Energy Strategy Reviews 24 (2019) 38–50.
24. N. Glanemann, S. N. Willner, A. Levermann, Paris climate agreement passes the cost-benefit test, Nature communications 11 (1) (2020) 1–11.
25. E. Kabir, P. Kumar, S. Kumar, A. A. Adelodun, K.-H. Kim, Solar energy: Potential and future prospects, Renewable and Sustainable Energy Reviews 82 (2018) 894–900.
26. P. Balakrishnan, M. S. Shabbir, A. F. Siddiqi, X. Wang, Current status and future prospects of renewable energy: A case study, Energy Sources, Part A: Recovery, Utilization, and Environ- mental Effects (2019) 1–6.
27. J. R. F. Diógenes, J. Claro, J. C. Rodrigues, M. V. Loureiro, Barriers to onshore wind energy implementation: A systematic review, Energy Research & Social Science 60 (2020) 101337.
28. M. Lange, A. M. O'Hagan, R. R. Devoy, M. Le Tissier, V. Cummins, Governance barriers to sustainable energy transitions–assessing ireland's capacity towards marine energy futures, Energy Policy 113 (2018) 623–632.
29. M. Hassan, M. K. Afridi, M. I. Khan, An overview of alternative and renewable energy governance, barriers, and opportunities in pakistan, Energy & Environment 29 (2) (2018) 184–203.

30. M. Gholikhani, R. Nasouri, S. A. Tahami, S. Legette, S. Dessouky, A. Montoya, Harvesting kinetic energy from roadway pavement through an electromagnetic speed bump, Applied Energy 250 (2019) 503–511.
31. H. Wang, A. Jasim, X. Chen, Energy harvesting technologies in roadway and bridge for different applications–a comprehensive review, Applied energy 212 (2018) 1083–1094.
32. K. Fan, M. Cai, H. Liu, Y. Zhang, Capturing energy from ultra-low frequency vibrations and human motion through a monostable electromagnetic energy harvester, Energy 169 (2019) 356–368.
33. K. Fan, Y. Zhang, H. Liu, M. Cai, Q. Tan, A nonlinear two-degree-of-freedom electromagnetic energy harvester for ultra-low frequency vibrations and human body motions, Renewable Energy 138 (2019) 292–302.
34. L. Zhang, H. Dai, Y. Yang, L. Wang, Design of high-efficiency electromagnetic energy harvester based on a rolling magnet, Energy Conversion and Management 185 (2019) 202–210.
35. Y. Pan, T. Lin, F. Qian, C. Liu, J. Yu, J. Zuo, L. Zuo, Modeling and field-test of a compact electromagnetic energy harvester for railroad transportation, Applied Energy 247 (2019) 309– 321.
36. J. W. Kim, M. Salauddin, H. Cho, M. S. Rasel, J. Y. Park, Electromagnetic energy harvester based on a finger trigger rotational gear module and an array of disc halbach magnets, Applied Energy 250 (2019) 776–785.
37. T. Asai, Y. Araki, K. Ikago, Energy harvesting potential of tuned inertial mass electromagnetic transducers, Mechanical Systems and Signal Processing 84 (2017) 659–672.
38. W. Ding, Z. Mao, H. Cao, K. Wang, Performance evaluation of a two-directional energy harvester with low-frequency vibration, Smart Materials and Structures 29 (5) (2020) 055006.
39. H. Azangbebil, S. Djokoto, M. Agelin-Chaab, E. Dragašius, A study of nonlinear piezoelectric energy harvester with variable damping using thin film mr fluid, IFAC-PapersOnLine 52 (10) (2019) 394–399.
40. J. Kim, S. Byun, S. Lee, J. Ryu, S. Cho, C. Oh, H. Kim, K. No, S. Ryu, Y. M. Lee, et al., Cost-effective and strongly integrated fabric-based wearable piezoelectric energy harvester, Nano Energy (2020) 104992.
41. L. L. Theng, M. A. Mohamed, I. Yahya, J. Kulothungan, M. Muruganathan, H. Mizuta, Piezo- electric energy harvester enhancement with graphene base layer, Materials Today: Proceedings 7 (2019) 792–797.
42. M. Rezaei, R. Talebitooti, S. Rahmanian, Efficient energy harvesting from nonlinear vibrations of pzt beam under simultaneous resonances, Energy 182 (2019) 369–380.
43. H. Parangusan, D. Ponnamma, M. A. A. Al-Maadeed, Stretchable electrospun pvdf-hfp/co-zno nanofibers as piezoelectric nanogenerators, Scientific reports 8 (1) (2018) 1–11.
44. A. Gaur, C. Kumar, S. Tiwari, P. Maiti, Efficient energy harvesting using processed poly (vinylidene fluoride) nanogenerator, ACS Applied Energy Materials 1 (7) (2018) 3019–3024.
45. O. Stetsovych, P. Mutombo, M. Svec, M. Samal, J. Nejedly, I. Cisarova, H. Vazquez, M. Moro- Lagares, J. Berger, J. Vacek, et al., Large converse piezoelectric effect measured on a single molecule on a metallic surface, Journal of the American Chemical Society 140 (3) (2018) 940–946.
46. L. Fetisov, D. Chashin, D. Saveliev, M. Afanas' ev, I. Simonov-Emel'yanov, M. Vopson, Y. Fetisov, Magnetoelectric direct and converse resonance effects in a flexible ferromagnetic- piezoelectric polymer structure, Journal of Magnetism and Magnetic Materials 485 (2019) 251–256.
47. O. K. Ignatius, A. E. I. E. Ibhaze, D. O. Dolapo, Renewable energy harvesting based on lead zirconate titanate crystal, International Journal of Engineering Technology and Sciences 6 (1) (2019) 131–146.
48. X. Shan, H. Li, Y. Yang, J. Feng, Y. Wang, T. Xie, Enhancing the performance of an underwater piezoelectric energy harvester based on flow-induced vibration, Energy 172 (2019) 134–140.
49. Y. Hu, B. Yang, X. Chen, X. Wang, J. Liu, Modeling and experimental study of a piezoelectric energy harvester from vortex shedding-induced vibration, Energy Conversion and Management 162 (2018) 145–158.
50. N. A. K. Z. Abidin, N. M. Nayan, M. M. Azizan, A. Ali, Analysis of voltage multiplier circuit simulation for rain energy harvesting using circular piezoelectric, Mechanical Systems and Signal Processing 101 (2018) 211–218.
51. S. P. Rajeev, S. K. John, R. Cherian, S. C. Karumuthil, S. Varghese, Next-generation rooftop tribo–piezo electric energy harvesting from rain power, Applied Nanoscience 10 (3) (2020) 679–686.
52. J.-C. Hsieh, D. T. Lin, C.-L. Lin, The development and optimization of an innovative piezoelec- tric energy harvester on the basis of vapor-induced vibrations, Mechanical Systems and Signal Processing 131 (2019) 649–658.
53. S. Balguvhar, S. Bhalla, Green energy harvesting using piezoelectric materials from bridge vibrations, in: 2018 2nd International Conference on Green Energy and Applications (ICGEA), IEEE, 2018, pp. 134–137.

54. S. Do Hong, K.-B. Kim, W. Hwang, Y. S. Song, J. Y. Cho, S. Y. Jeong, J. H. Ahn, G.-H. Kim, H. Cheong, T. H. Sung, Enhanced energy-generation performance of a landfilled road capable piezoelectric harvester to scavenge energy from passing vehicles, Energy Conversion and Management (2020) 112900.
55. S. Y. Jeong, W. S. Hwang, J. Y. Cho, J. C. Jeong, J. H. Ahn, K. B. Kim, S. Do Hong, G. J. Song, D. H. Jeon, T. H. Sung, Piezoelectric device operating as sensor and harvester to drive switching circuit in led shoes, Energy 177 (2019) 87–93.
56. Z. Li, T. Li, Z. Yang, H. E. Naguib, Toward a 0.33 w piezoelectric and electromagnetic hybrid energy harvester: Design, experimental studies and self-powered applications, Applied Energy 255 (2019) 113805.
57. G. J. Song, J. Y. Cho, K.-B. Kim, J. H. Ahn, Y. Song, W. Hwang, S. Do Hong, T. H. Sung, Development of a pavement block piezoelectric energy harvester for self-powered walkway applications, Applied Energy 256 (2019) 113916.
58. S. Asano, S. Nishimura, Y. Ikeda, T. Morita, H. Hosaka, Energy harvester for safety shoes using parallel piezoelectric links, Sensors and Actuators A: Physical (2020) 112000.
59. F. Qian, T.-B. Xu, L. Zuo, Design, optimization, modeling and testing of a piezoelectric footwear energy harvester, Energy conversion and management 171 (2018) 1352–1364.
60. P. Chaudhary, P. Azad, Energy harvesting using shoe embedded with piezoelectric material, Journal of Electronic Materials (2020) 1–10.
61. C. A. Soriano-Rangel, W. He, F. Mancilla-David, R. Ortega, Voltage regulation in buck-boost converters feeding an unknown constant power load: An adaptive passivity-based control, IEEE Transactions on Control Systems Technology (2020).
62. S. Ahmadzadeh, G. A. Markadeh, F. Blaabjerg, Voltage regulation of the y-source boost dc–dc converter considering effects of leakage inductances based on cascaded sliding-mode control, IET Power Electronics 10 (11) (2017) 1333–1343.
63. S. Kumari, S. S. Sahu, B. Gupta, Efficient sshi circuit for piezoelectric energy harvester uses one shot pulse boost converter, Analog Integrated Circuits and Signal Processing 97 (3) (2018) 545–555.
64. N. D. Nguyen, D. T. Bui, P. H. Truong, G.-M. Jeong, Classification of five ambulatory activities regarding stair and incline walking using smart shoes, IEEE Sensors Journal 18 (13) (2018) 5422–5428.
65. I. Snihir, W. Rey, E. Verbitskiy, A. Belfadhel-Ayeb, P. H. Notten, Battery open-circuit voltage estimation by a method of statistical analysis, Journal of Power Sources 159 (2) (2006) 1484– 1487.
66. Y. Su, C. Dagdeviren, R. Li, Measured output voltages of piezoelectric devices depend on the resistance of voltmeter, Advanced Functional Materials 25 (33) (2015) 5320–5325.
67. H. Jabbar, S. D. Hong, S. K. Hong, C. H. Yang, S. Y. Jeong, T. H. Sung, Sustainable micro- power circuit for piezoelectric energy harvesting tile, Integrated Ferroelectrics 183 (1) (2017) 193–209.
68. A. A. Chand, A. S. Arefin, F. Islam, K. A. Prasad, S. Singh, M. Cirrincione, K. A. Mamun, Design simulation of a novel fluid based footstep energy harvesting system, Sustainable Energy Technologies and Assessments 39 (2020) 100708.